# Zinc Nucleation and Growth in Microgravity

B. Patrick Michael* and J. A. Nuth III†

*Code 691, NASA-Goddard Space Flight Center, Greenbelt, MD 20771*

L. U. Lilleleht

*Department of Chemical Engineering, University of Virginia, Charlottesville, VA 22904*

(March 20, 2000)

## Abstract

We report our experiences with zinc nucleation in a microgravity environment aboard NASA's Reduced Gravity Research Facility. Zinc vapor is produced by a heater in a vacuum chamber containing argon gas. Nucleation is induced by cooling and its onset is easily detected visually by the appearance of a cloud of solid, at least partially crystalline zinc particles. Size distribution of these particles is monitored *in situ* by photon correlation spectroscopy. Samples of particles are also extracted for later analysis by SEM. The initially rapid increase in particle size is followed by a slower period of growth. We apply Scaled Nucleation Theory to our data and find that the derived critical temperature of zinc, the critical cluster size at nucleation, and the surface tension values are all in reasonably good agreement with their accepted literature values.

Typeset using REVTEX

*National Research Council Research Associate

†Author to whom correspondence should be addressed

## I. INTRODUCTION

Thermally induced convection has always been a complicating factor in studies of refractory materials nucleation[1]. In this paper we report the first attempts to conduct refractory nucleation experiments under conditions where thermally induced convection does not occur, namely in the microgravity environment of NASA's Reduced Gravity Research Facility. These experiments were conducted as part of a long-term program to study the physical and optical properties of well-characterized refractory particulate clouds during nucleation and coagulation processes. Such clouds would be much simpler analogs of the more complex natural systems found in circumstellar outflows, in protostellar nebulae, or in volcanic eruptions.

In Section II we will briefly describe the experimental system and the conduct of the experiments aboard the Reduced Gravity Research Facility. Section III will present and discuss the results of the nucleation experiments, while Section IV will discuss the evolution with time of the particle size distribution following nucleation. We will show that zinc nucleation appears to follow Scaled Nucleation Theory[2] predictions more closely than those of Classical Nucleation Theory[3]. We will also show that the growth of zinc particulates appears to be an extremely inefficient process. This latter phenomenon is consistent with the morphology of the condensate phase: well-ordered, turned, hexagonal platelets.

## II. EXPERIMENTAL APPARATUS AND OPERATION

While an abbreviated version of the experimental apparatus and its operation aboard NASA's Reduced Gravity Research Facility has recently been published[4], a more detailed description of it is available elsewhere[5].

The heart of the system is a cylindrical vacuum chamber containing inert gas, in our case argon with a small percentage of hydrogen. The chamber is divided into two sections as shown by the schematic drawing in Figure 1. Zinc vapors are produced in the heated

crucible just below the opening in the vapor shield. Nucleation takes place in the upper section of the chamber which is devoid of any extraneous surfaces close to the vapor entrance to minimize the possibility of particle formation via heterogeneous nucleation. There are eight vacuum ports located concentrically around this upper section: for the laser light scattering system, the particle extraction system, the video camera and its light source, and for the vacuum pump and inert gas pressure control connections. The lower section houses a thermally and electrically insulated graphite heater, and is provided with feed-throughs for high current electrical power and for the 20 thermocouples to monitor temperatures throughout the chamber. Thermocouples are placed within the heater and embedded in the heat shield as well as along the walls of the upper section of the vacuum chamber. Data from these thermocouples provide the boundary values needed for calculations of the temperature field within the chamber as a function of time. Chamber pressure, acceleration levels, thermocouple data, and the light scattering information are all recorded during the experiments using a computerized data acquisition system.

Photon Correlation Spectroscopy (PCS) is employed to follow the growth of particles using a 10mW solid-state diode laser beam launched through a single-mode fiber optics system into the region of interest at $\sim$2.5 cm above the center of the crucible. A second fiber optics system "captures" the scattered light orthogonally from the original laser beam and routes this signal to an EG&G Single Photon Counting Module (SPCM). The output of the SPCM is used to generate an autocorrelation function from which the particle size distribution is extracted using a Maximum Entropy Method[6]. This distribution is representative of particles only within a cubic volume of approximately 1 millimeter on a side located along the centerline of the crucible 2.5 cm above it. The onset of nucleation is detected by monitoring the region above the crucible with a CCD-based video system. Detection of light scattered at 90° by the growing zinc particles is a sensitive indicator of the presence of solid grains. A frame-by-frame comparison of the recorded video images provides a relatively precise indication of the onset of nucleation as can be seen in Figure 2.

The NASA Reduced Gravity Research Facility is a KC-135 aircraft – a specially modified

Boeing 707 jet capable of flying parabolic trajectories designed to produce short periods of effectively reduced levels of gravitational acceleration. In our experiments we bring our zinc crucible close to working temperatures as the KC-135 climbs to an appropriate altitude (typically 25,000 feet) over the Gulf of Mexico. The ambient argon gas pressure in the chamber is then brought down from 200 torr to the working pressure of the experiment using our vacuum pump, and the temperature of the crucible is increased to the desired value. As the aircraft begins its climb along the upward leg of a parabolic trajectory, the acceleration level reaches approximately 1.8 $g$ prior to the inflection point. After this point the apparent gravitational acceleration is reduced to approximately $10^{-3}g$ as the aircraft follows a ballistic path which peaks at about 35,000 feet. The nearly weightless period continues until the aircraft crosses the second inflection point on the downward leg of the parabola and pulls out, again at an acceleration peaking at 1.8 $g$. Following several seconds of level (1 $g$) flight, the KC-135 begins accelerating into the next parabolic maneuver. Usually after 10 parabolas the experimenters have 2-3 minutes of level flight as the aircraft turns around to get into position to begin the next series of parabolas. During this time the vacuum pump can be turned on to pump down the particle collection system in preparation for sample extraction or for chamber gas pressure adjustment, if desired. The pump must be turned off and sealed before the start of each series of parabolas in order to keep the pump oil in place.

The data collection system is activated prior to the first parabola and continues operating throughout the flight which may have as many as 40 parabolas. Similarly, the video camera is also turned on prior to the first parabola to monitor and record the conditions in the chamber continuously. A particle collection system is operated periodically as needed during the flight. The particle collector is normally stored behind a gate valve attached to one of the concentric ports. The collector is deployed by opening the gate valve and pushing its head into the center of the chamber using a push-pull feed-through. The SEM stubs attached to the collector head are exposed to the particle cloud for specific periods of time and then withdrawn behind the gate valve to avoid contamination. The SEM stubs can be removed

and replaced by new ones as the KC-135 changes course between each set of 10 parabolas. An example of typical zinc particles collected *in situ* using this collection system is shown in Figure 3.

Temperature data are collected from the following sources: from within the zinc crucible and at the throat of the opening into the upper chamber, at 9 positions in line on the vapor shield separating the upper and lower sections of the chamber, at 5 positions along the outer wall of the upper section, at several points along the top and bottom of the upper section, and at the junction of the thermocouple feed-throughs. A numerical code has been developed to compute the temperatures at any position throughout the upper section of the chamber. This model makes use of measured temperatures along its periphery as boundary values, and accounts for both energy and mass transport as a function of time and local acceleration[7,8]. Temperatures near the measured boundary points are predicted quite accurately by this model as demonstrated by calibration runs in which additional thermocouples had been placed at various locations within the chamber. However, these calibrations showed also that actual temperatures in the central portion of the chamber could deviate by as much as 20-100 K from the computed model values, especially during brief transient events such as going from zero to 1.8 $g$. Under most conditions of the calibration runs the model temperatures at the point of the laser light scattering measurements ($\sim$2.5 cm above the crucible opening) consistently overestimated the measured temperatures by approximately 20-30 K once the transients from rapid changes in acceleration had settled, i.e. after $\sim$3 to 5 seconds.

## III. RESULTS OF ZINC NUCLEATION EXPERIMENTS

During the 1.8 $g$ acceleration period, while climbing into the parabolic portion of the flight trajectory, zinc vapor leaving the crucible is tightly columnated by strong convective currents and does not produce particles observable by our video system. It is also possible that the zinc vapor is too dense to leave the crucible during the 1.8 $g$ pullup phase. In either

case no zinc particles are observed during the high-g portion of any of the experiments as shown in Figure 4. Just after the onset of 0 $g$ the previously vigorous convection rapidly dies away and the zinc vapor slowly forms a growing bubble-like cloud of differing optical density over the throat of the crucible, the outline of which is easily visible by eye. At a time between 5 to 10 seconds after the onset of 0 $g$, spontaneous nucleation is observed at the slowly expanding vapor bubble's outer boundary and the process progresses rapidly to the interior of the bubble. The entire nucleation event takes less than 0.2 seconds, although particle growth continues for slightly longer. Figure 2 shows a sequence of six successive frames of video recorded at 30 frames per second. Data from each of the parabolas in which zinc was observed to nucleate is analyzed below.

Several important assumptions are made in this analysis which should be noted first. The flux of particles is assumed to be essentially constant over the temperature range studied, and we do not account for any possible effects from the heat of condensation of the zinc particles on the ambient gas. Also, the partial pressure of zinc vapor within the hemispherical bubble, which appears at 0 $g$, is assumed to be the same as its vapor pressure at the crucible (source) temperature. We base these assumptions on the following: (i) the vapor pressure of zinc at the source is slightly higher ($\sim$29 torr) than the ambient gas pressure ($\sim$26 torr) in the nucleation section of the chamber, and (ii) the density of zinc vapor is considerably greater than that of the ambient argon gas and is assumed to displace the argon within the expanding zinc bubble.

The measured temperature at the crucible (source) and the calculated condensation temperatures (as described above) are used to estimate the equilibrium vapor pressures and the supersaturation ratios. Vapor pressures, in atmospheres, are obtained from published zinc vapor pressure data[9] using the following equation:

$$\ln P_v = -\frac{A}{T} + B \ln T + CT + D \qquad (1)$$

where $T$ is the absolute temperature and $A$, $B$, $C$ and $D$ are the Antoine coefficients listed for zinc in Table I. Finally, the equilibrium vapor pressure values are used to calculate

supersaturation ratios

$$S = P_{\text{source}}/P_{\text{equilibrium}} \tag{2}$$

where $P_{\text{source}}$ is the equilibrium vapor pressure at the crucible (source) temperature and $P_{\text{equilibrium}}$ is the equilibrium vapor pressure at points along the observed boundary of the nucleation front.

We note that, although nucleation takes place all along the zinc vapor cloud/ambient argon gas interface simultaneously, there is only one source temperature, i.e. the crucible temperature, for all of the zinc vapor. The source pressure must be just slightly higher than that of the ambient gas since we observe the zinc bubble expanding only slowly into the upper chamber. This line of reasoning is totally consistent with our observation that "bubbles" form when the crucible temperature is high enough for the vapor pressure of zinc there to exceed the pressure of the ambient argon gas, whereas no "bubbles" are observed when the zinc vapor pressure in the crucible is less than the pressure of the argon gas.

Because of the model temperature uncertainties noted previously and because each zinc "bubble" is presumably zinc vapor at a uniform pressure determined by the crucible temperature, each "bubble" is used to extract only one "best" data point. This data point is selected closest to the thermocouple grid laid out radially around the crucible opening. Agreement between the model temperatures and reality there, based on our calibration runs, is expected to be better than 5 K. Only "bubbles" with a sharp, clearly delineated particle cloud/ambient gas interface are useful for analysis. The position where this interface is clearest is usually along the lower right or left of the cloud boundary and close to thermocouples fixed on the vapor shield. Since that is usually within 0.1 cm of a measured boundary temperature location, we expect nucleation temperatures calculated from our model to be quite accurate.

Classical Nucleation Theory predicts that the particle formation rate, $J$, should be related to the supersaturation ratio, $S$, and the temperature, $T$, by the following relationship[10]:

$$J = \left(\frac{2\sigma}{\pi m}\right)^{1/2} V N_1^2 \exp\left[\frac{-16\pi\sigma^3 V^2}{3k^3T^3(\ln S)^2}\right] \tag{3}$$

where $\sigma$ is the surface free energy, $m$ is the mass of the condensing molecule, $V$ is the volume of the condensing monomer molecule, $N_1$ is the number density of the monomer, and $k$ is the Boltzmann's constant. Equation 3 can be rearranged into the following form:

$$\frac{C_2\sigma^3}{T^3\left(\ln S\right)^2} + \ln\left(\frac{J}{C_1\sigma^{1/2}}\right) = \ln\left(N_1^2\right) \tag{4}$$

where

$$C_1 = \left[\frac{2V^2}{\pi m}\right]^{1/2} \tag{5}$$

and

$$C_2 = \frac{16\pi V^2}{3k^3}. \tag{6}$$

With this rearrangement, a plot of $\left[T^3\left(\ln S\right)^2\right]^{-1}$ versus $\ln\left(N_1^2\right)$ should yield a straight line if $\sigma$ remains approximately constant over the temperature range explored. An average value for $\sigma$ can then be obtained from the slope of the line provided that the monomer volume can be estimated. Figure 5 is such a plot for our data.

Forcing a straight line fit to Figure 5 gives a slope of 5.2 x $10^{-10}$ with an intercept of 107.3 and the correlation coefficient a low 0.14. The surface tension derived from this slope is 0.33 $N/m$ which is a surprisingly good match to the accepted value of 0.75 $N/m$. However, the flux calculated using our data is 8.6 x $10^{29}$ particles $m^{-3}s^{-1}$. Given that the average final particle size derived from PCS data, as discussed in Section IV, is about 130 nm, this calculated flux value is physically impossible. A flux of just 6.6 x $10^{28}$ particles $m^{-3}s^{-1}$ of 130 nm particles is equivalent to a solid block of zinc! As the zinc vapor pressure was typically 30 torr, the high particle flux derived above from the Classical Nucleation Theory and Figure 5 is clearly in error.

The critical cluster size can be obtained in Classical Nucleation Theory by setting the change in free energy ($\Delta G$) with respect to the radius ($r$) equal to zero. This then leads to an equation for the critical cluster radius of the form[10]

$$r_c = \frac{2\sigma M}{RT\left(\ln S\right)\rho}, \tag{7}$$

where $r_c$ is the critical radius, $\sigma$ is the surface free energy, $M$ is the molar mass, $R$ is the gas constant, $T$ is the temperature and $\rho$ is the material density. Using the surface tension derived from Figure 5, Equation 7 yields a critical cluster radius of (0.93 to 1.2) x $10^{-10}m$ for the range of temperatures in our experiments. These values are also unrealistic since the radius of a single zinc atom is approximately 1.5 x $10^{-10}m$, i.e. larger than the cluster size. We therefore conclude that Classical Nucleation Theory does not provide a good description of the nucleation of zinc vapor as observed in our experiments.

The Classical Nucleation Theory was developed primarily to predict droplet formation in vapors of volatile substances such as water or ethanol, whereas the Scaled Nucleation Theory[2] was intended to apply to a much wider range of materials. In Scaled Nucleation Theory all of the material properties are scaled to their values at the critical point. For a flux of 1 particle $cm^{-3}s^{-1}$, Scaled Nucleation Theory predicts the following relationship between the critical supersaturation ratio, $S_{cr}$, and the condensation temperature, $T$, for temperatures well below the critical temperature of the material:

$$\ln S_{cr} \approx \Gamma \Omega^{3/2} \left[\frac{T_c}{T} - 1\right]^{3/2} \tag{8}$$

where $T_c$ is the critical temperature of the material while $\Gamma$ is a weak function of temperature and supersaturation and has an approximate value of 0.53. The quantity $\Omega$ here denotes the negative partial derivative of the surface tension per molecule with respect to the temperature and typically ranges from 1.5 for associated liquids to a maximum of 2.2 for solids. For fluxes larger than 1 particle $cm^{-3}s^{-1}$, the critical supersaturation is modified as follows:

$$\ln S \approx \ln S_{cr} \left[1 + \frac{\ln J}{(2 \ln J_{cr})}\right] = Q \ln S_{cr}, \tag{9}$$

where the term $\ln(J_{cr})$ is equal to $72 \pm 3$ and $Q$ represents the bracketed term.

One of the predictions of Scaled Nucleation Theory is that a plot of $(\ln S)^{2/3}$ vs $T^{-1}$ should yield a straight line with a slope which, when divided by the negative of the intercept, will give the critical temperature of the material. We follow this procedure and find the slope and the intercept of the straight line in Figure 6 to be 3895 and -1.887, respectively. These yield

for zinc a critical temperature of 2064 K which is in good agreement with 1967 K obtained from a commonly used "rule of thumb" method for estimation of the critical temperature of a substance by dividing its boiling point temperature by 0.6.

A critical cluster size can be calculated from particle flux and the supersaturation values. Although we did not measure the nucleation flux directly, a good estimate for this parameter would be approximately $10^{14}$ particles $m^{-3}s^{-1}$. According to Scaled Nucleation Theory, the critical cluster size, $n_{cr}$, is

$$n_{cr} = \left[\frac{2A}{3B}\right]^3 \tag{10}$$

where

$$A = (36\pi)^{1/3}\,\Omega\left[\frac{T_c}{T} - 1\right] \tag{11}$$

and

$$B = \ln S. \tag{12}$$

Assuming a constant $\Gamma$ of 0.53 and a flux of $10^{14}$, Equations 11 and 12, together with our measured supersaturations and the critical temperature derived above, yield a value for $\Omega$ of 2.66. This is unfortunately higher than the 1.5 to 2.2 range found from other applications of Scaled Nucleation Theory. However, using our derived value for $\Omega$, Equation 10 yields a value for the number of atoms in the critical cluster that varies from 6 to 9 over the range of our experiments. The critical cluster sizes from Scaled Nucleation Theory are physically realistic and more believable than those from the Classical Nucleation Theory even though they are slightly smaller than those seen in other refractory work. The smaller cluster size may be explained by the extremely high supersaturations in our experiments. In most refractory experiments the natural logarithms of the supersaturation ratios vary from approximately 3 to 6, while in our work these are much higher ranging from 10 to 19.

One commonly given reason why Scaled Nucleation Theory appears to provide better agreement between experiments and theory is that by using scaled quantities it is able

to extend the useful range of the Classical Theory. Bulk liquid surface tension and bulk number density, $\rho$, do not appear explicitly in the Scaled Nucleation Theory — rather they are combined as a ratio shown on the left side of the equation given by Ferguson *et al.*[11] and replaced in the scaled formalism with the quantity $\Omega$:

$$\frac{\sigma}{k\rho^{2/3}} = \Omega\,[T_c - T]\,. \tag{13}$$

Once the value of $\Omega$ is known, Equation 13 can be rearranged to give the effective surface energy. Using the bulk liquid density of zinc for $\rho$ along with our values of $\Omega$ and $T_c$ an expression for $\sigma$ becomes:

$$\sigma = 1.262 - 6.115\text{x}10^{-4}T. \tag{14}$$

Thus at the melting point of zinc Equation 14 predicts an effective surface tension of 0.84 $N/m$. This is within 10% of the accepted value of 0.75 $N/m$. Scaled Nucleation Theory, therefore, appears to offer a better description of our experiments than does Classical Nucleation Theory.

## IV. GROWTH OF ZINC PARTICLES

The laser light scattering system is designed to collect information on the size distribution of particles in a sample volume of approximately 1 $mm^3$ at a height of 2.5 cm above the crucible opening along the centerline of the cylindrical chamber. In general, particles such as those seen in Figure 3, are not those whose size distribution is measured by the light scattering system. This is because the particle extraction and light scattering measurements cannot be performed simultaneously as one effectively blocks the other. We assume that most particles formed at the same time will grow by similar degrees and so the measured size distributions should be typical of the average particle size distribution in the system.

Figures 7 and 8 show the developing particle size distributions from two parabolas exhibiting zinc nucleation. The distributions are computed for every 0.05 seconds following

the first appearance of zinc particles on the video system. Both sets of data show a rapid initial growth of zinc particles followed by a much slower growth period after approximately 0.20 seconds. Size distributions measured approximately 10-15 seconds after the initiation of nucleation show the particles to have grown to mean diameters of 141 nm and 152 nm, respectively. It seems clear that the rapid initial growth is fueled by the relatively high local concentration of zinc vapor which is depleted within roughly 0.20 seconds following the appearance of condensation nuclei. The additional growth to 140-150 nm occurs much more slowly and could be due to the diffusion of zinc vapor from the crucible to the growing particles.

Table II summarizes the data and calculations on the growth of zinc particles shown in Figures 7 and 8 from the two parabolas at slightly different temperatures and pressures. The results from both of these sets are quite similar: the number of atoms of zinc added to the average growing grain in any given time interval is very roughly proportional to the surface area of the grain, but it is much lower than the maximum number of atoms that could have been added if every collision of a molecule from the vapor with the particle surface had resulted in capture and hence in particle growth.

Consider as an example the second case in Table II where the temperature is 519 K and the zinc source partial pressure is 29.8 torr. According to Equation 15 there are

$$\mu = \frac{P}{(2\pi mkT)^{1/2}} \tag{15}$$

or roughly 5.6 x $10^7$ collisions per $s^{-1}$ per $nm^2$ using a mass of 1.1 x $10^{-25}$ kg for zinc atoms. Thus roughly 3 x $10^6$ collisions occur per $nm^2$ in the 0.05 second time interval between calculation of each particle size distribution, yet only on the order of $10^7$ zinc atoms are added to the entire grain during that same period. The average surface area of the zinc grains is on the order of $10^5$ $nm^2$ and approximately 3 x $10^{11}$ zinc atoms collided and could have been added during the 0.05 second time interval. The efficiency of the growth of these particles is therefore approximately 0.003% or less – an extremely low, and at first sight very surprising result given the rapid depletion of the vapor.

However, since zinc melts at only 419 K and we find nucleation at temperatures of less than approximately 520 K, it is possible that much of the growth of the zinc particles occurs at even lower temperatures. An examination of the zinc particles collected *in situ*, Figure 3, reveals hexagonal grains turned perpendicular to the c-axis: in cross-section these grains look like small bow ties. If growth takes place below the melting point of zinc, then a zinc atom impinging on the growing surface would need to find an appropriate crystalline defect before attachment to the surface could take place. Formation of crystalline particles, as they appear to be in Figure 3, certainly suggests that this could have been the case. Such a process would be relatively inefficient when compared with the growth of a liquid droplet. But how likely is it that growth takes place at such low temperatures?

First, we note that zinc nucleation temperatures used in our analyses come from near the bottom of the zinc vapor cloud and are closest to the grid of boundary thermocouples. We are, therefore, quite comfortable about the accuracy of the temperature at which these grains nucleate. However, the light scattering measurements used to determine the particle size distributions are made 2.5 cm above the crucible and are therefore somewhat distant from any measured boundary temperatures. As noted previously, temperatures at this location were typically at least 20-30 K lower than what our model calculations produced, and the temperature field at the lower (crucible) boundary was always higher than the temperature above the crucible. For the cases shown in Figures 7 and 8 the model temperatures at the location of the light scattering measurements were 447 K and 519 K, respectively. Given these uncertainties in the temperatures where the particle size distributions measurements are made and the fact that the model temperatures are upper limits to the actual temperatures, we feel quite certain that growth of zinc particles proceeds directly from the vapor to the crystalline solid without an intermediary liquid state. This then could also explain the relatively inefficient growth we observed.

## V. CONCLUSIONS

Our experiments demonstrate that the Scaled Nucleation Theory provides a better description of zinc nucleation than does the Classical Nucleation Theory. Based on our experimental data and the Scaled Nucleation Theory we derive a value for the critical temperature of zinc vapor of 2064 K and a surface tension at the melting point of 0.84 N/m, both of which are close to the published literature values. We also find that the growth of zinc particles takes place by direct deposition from vapor onto at least partially crystalline solid grains. This process is extremely inefficient with fewer than 3 collisions in $10^5$ resulting in addition of an atom to the growing grain.

# REFERENCES


[1] J. A. Nuth and F. T. Ferguson. Nucleation of solids from the gas phase. In M. C. Weinberg, editor, *Ceramic Transactions*, page 23, Westerville, OH 43081, 1993. The American Ceramic Society.

[2] B. N. Hale. Application of scaled homogeneous Nucleation-Rate formalism to experimental data at $t \ll t_c$. *Physical Review A*, 33:4156, 1986.

[3] R. Becker and W. Döring. Kinetische behandlung der keimbildung in übersättigten dämpfen. *Annalen der Physik*, A125:719, 1935.

[4] B. P. Michael, J. A. Nuth III, L. U. Lilleleht, E. Bussoletti, L. Colangeli, and P. Palumbo. A nucleation experiment in low gravity conditions: Monitoring and collection of mg and zn particles. *Advances in Space Research*, 24:1273, 1999.

[5] B. P. Michael. *Characterization of Refractory Particulates Using Light Scattering Methods in a Microgravity Environment.* PhD Dissertation, University of Virginia, 1998.

[6] S. Nyeo and B. Chu. Maximum-Entropy analysis of photon correlation spectroscopy data. *Macromolecules*, 22:3998, 1989.

[7] F. T. Ferguson. *Numerical Simulation of Natural Convection Flows Within a Nucleation Chamber Under Variable Gravity.* PhD Dissertation, University of Virginia, 1993.

[8] F. T. Ferguson, L. U. Lilleleht, J. A. Nuth III, and J. R. Stephens. Microgravity nucleation of refractory materials: Modeling of transport processes in the nucleation chamber. *Chemical Engineering Communications*, 125:63, 1993.

[9] D. R. Gaskell. *Introduction to Metallurgical Thermodynamics, 2nd Edition.* Hemisphere Publishing Corporation, New York, 1981.

[10] A. W. Adamson. *Physical Chemistry of Surfaces (5th Edition).* John Wiley & Sons, Inc., New York, 1990.

[11] F. T. Ferguson, J. A. Nuth III, and L. U. Lilleleht. Experimental studies of the vapor phase nucleation of refractory compounds. IV. the condensation of magnesium. *J. Chem. Phys.*, 104:3205, 1996.

## FIGURES

FIG. 1. Cross-sectional Diagram of the Nucleation Chamber

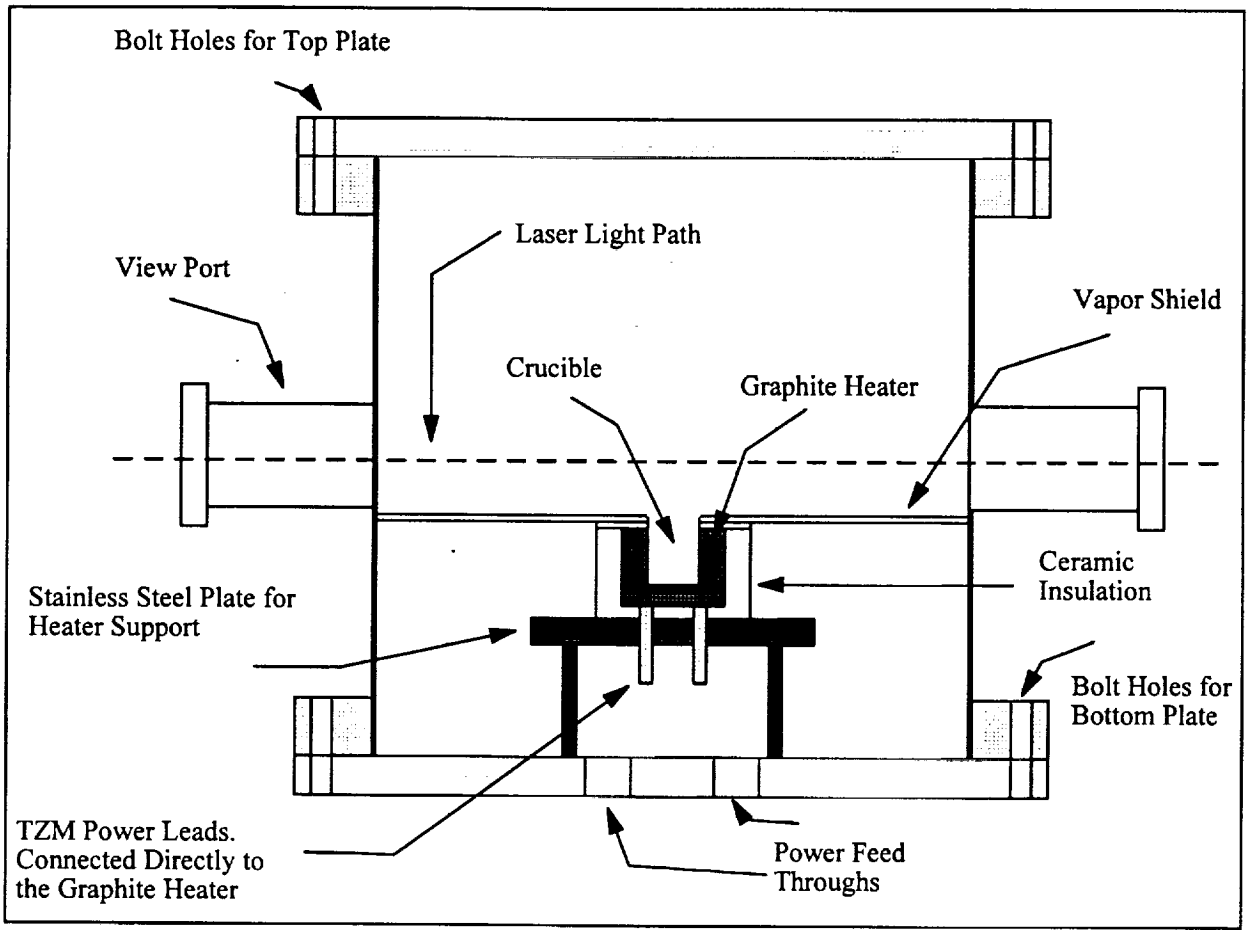

FIG. 2. Series of Frames for the Nucleation Event

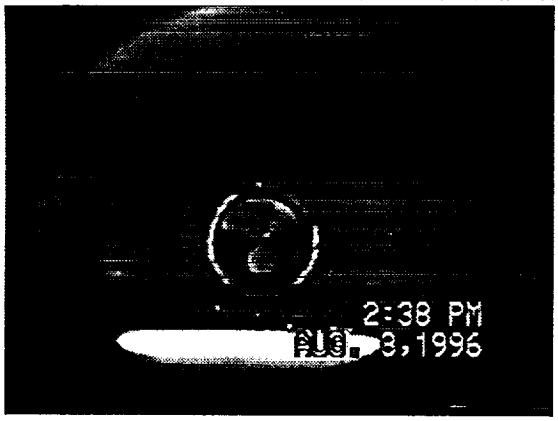


(a) Frame Before Nucleation Begins

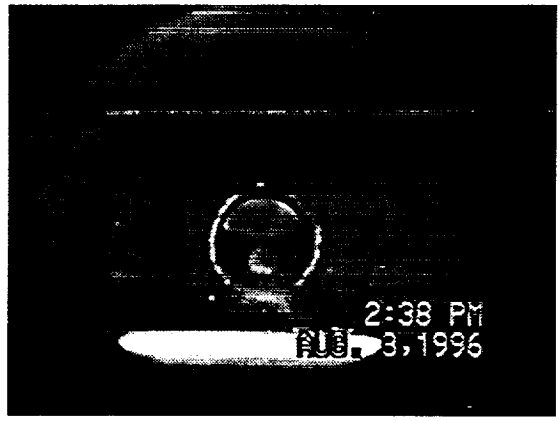


(b) Start of Nucleation

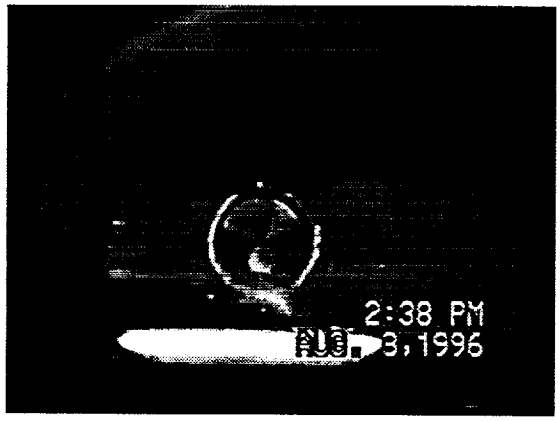


(c) 1/30 Second Later

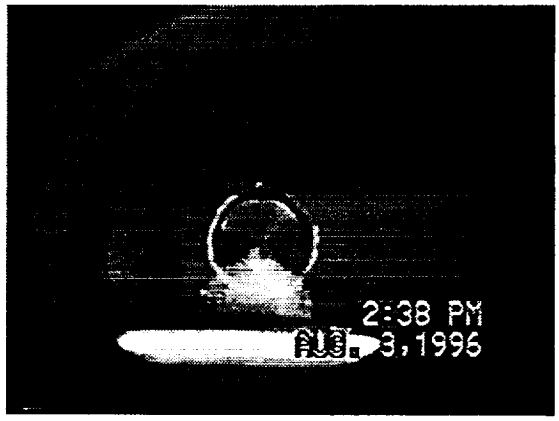


(d) 2/30 Second Later

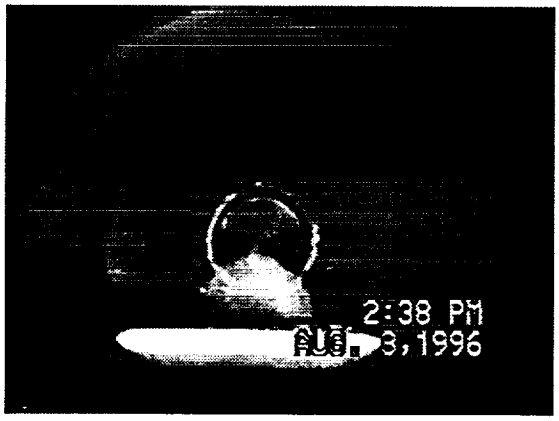


(e) 3/30 Second Later

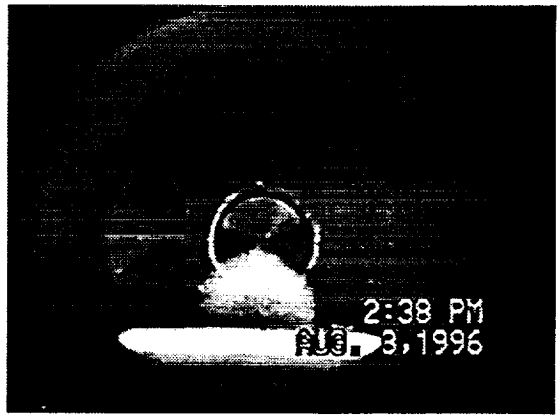


(f) 4/30 Second Later

FIG. 3. Zinc Particles Collected *in situ*

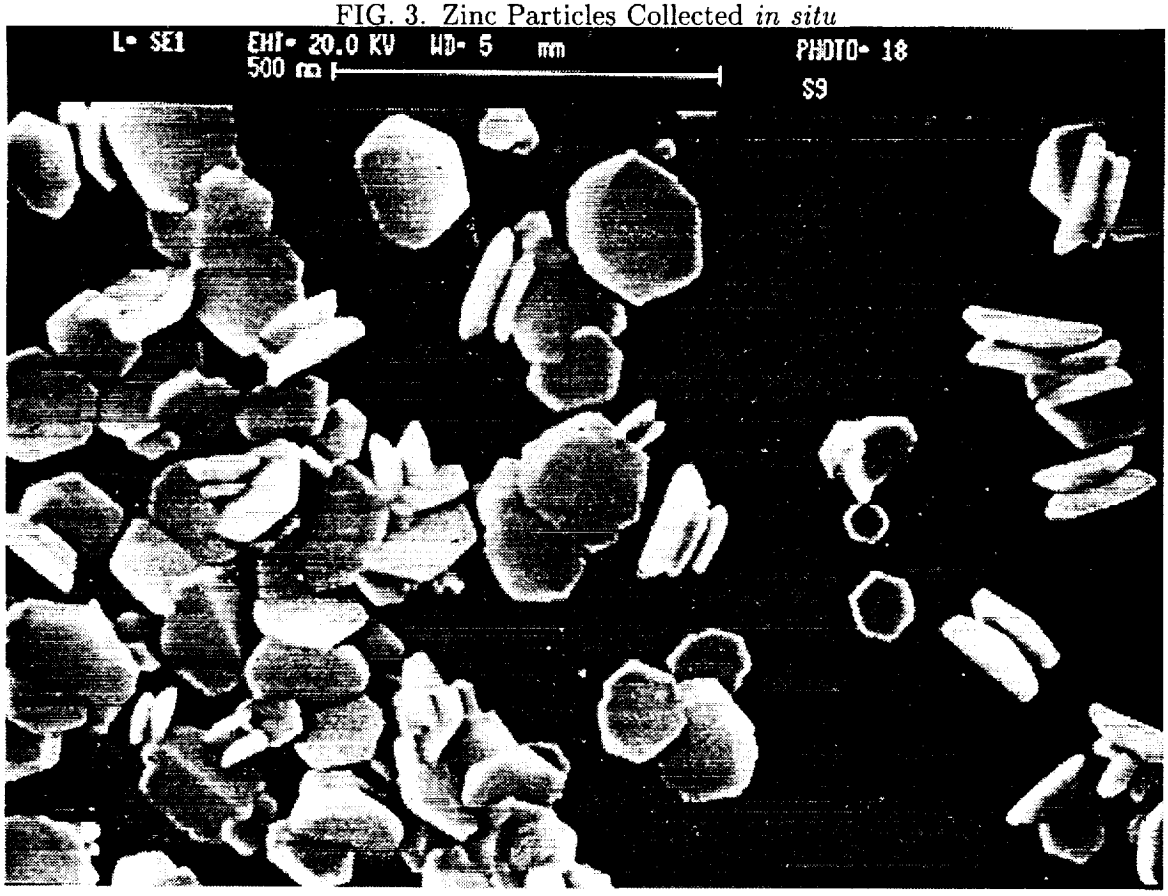


FIG. 4. Zinc Vapor in High G

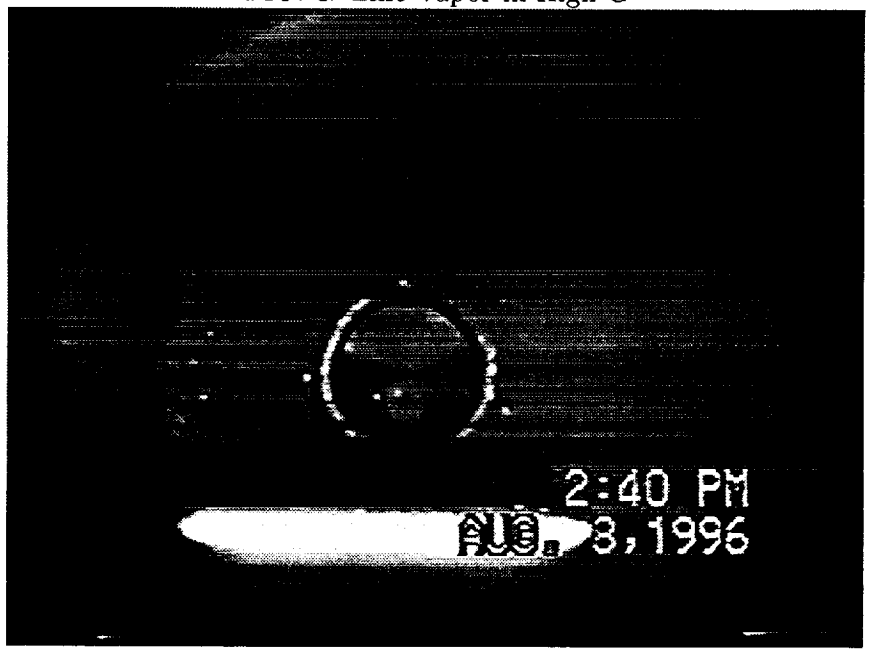

FIG. 5. Plot of $\left(T^3 (\ln S)^2\right)^{-1}$ versus $\ln\left(N_1^2\right)$ for Case 1

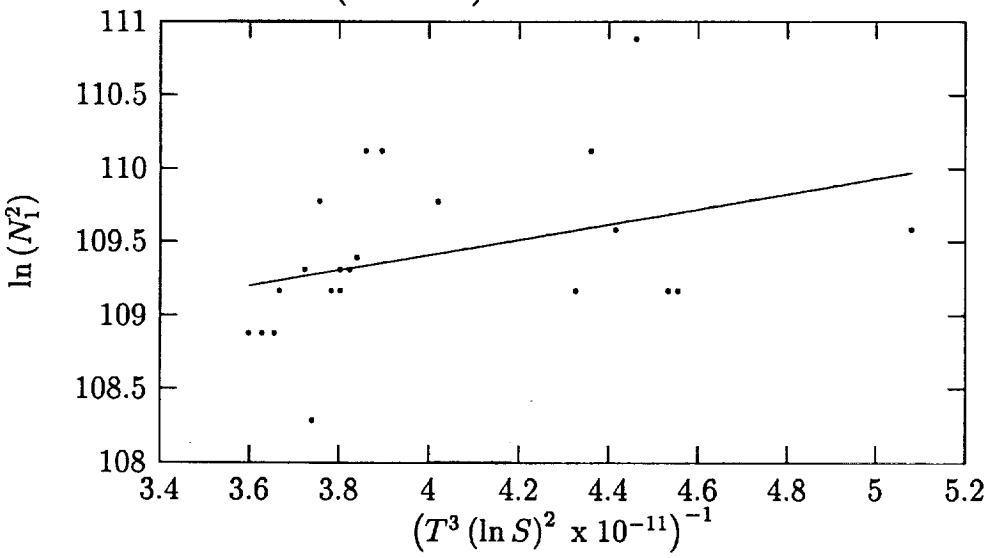


FIG. 6. Plot of $(\ln S)^{2/3}$ versus $1/T$ in Accordance with Scaled Nucleation Theory

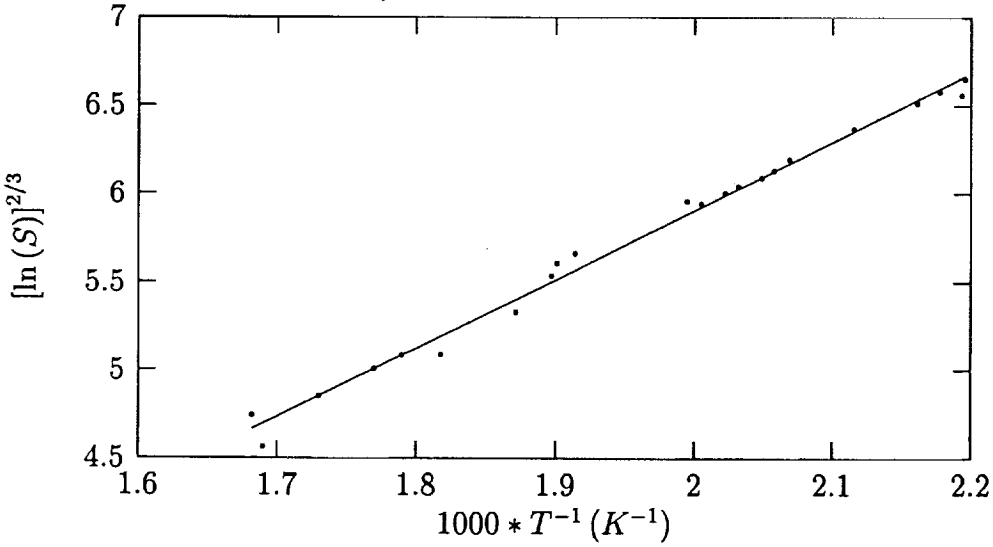

FIG. 7. Zinc Particle Size During Nucleation (Example 1)

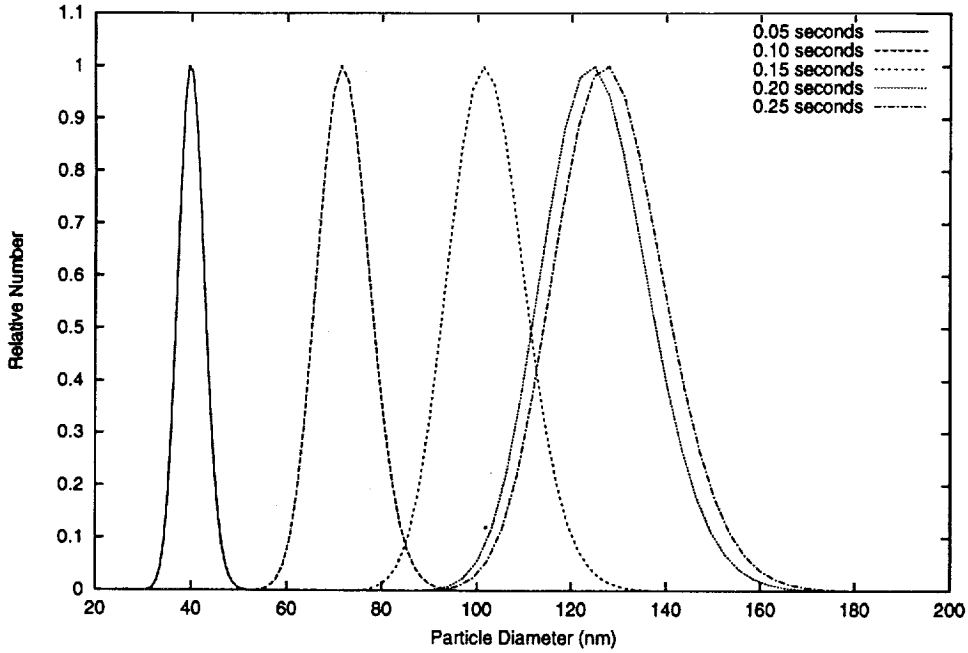


FIG. 8. Zinc Particle Size During Nucleation (Example 2)

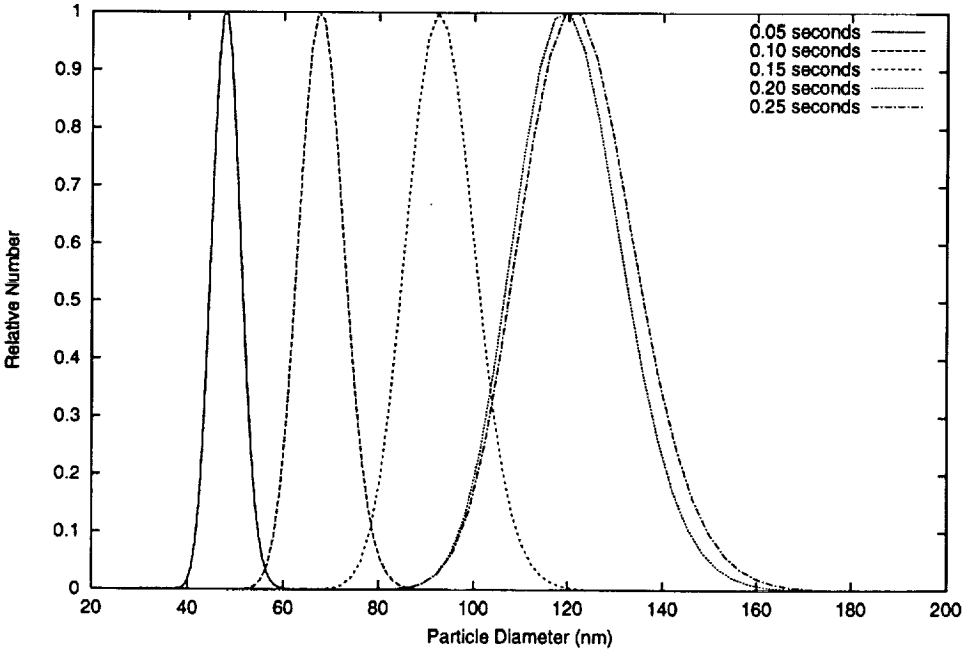

# TABLES

TABLE I. Antoine Equilibrium Vapor Pressure Coefficients for Zinc

| A | B | C | D | T(K) Range |
|---|---|---|---|---|
| 15780.0 | -0.755 | 0.0 | 19.25 | 273 - $T_{mp}$ |
| 15250.0 | -1.255 | 0.0 | 21.79 | $T_{mp}$ - 1180 |

TABLE II. Growth Data for the Zinc Particles Shown in Figures 7 and 8

| | time(s) | Diameter (nm) | Surface Area ($10^4$)nm$^2$ | Volume (nm$^3$) | # atoms ($10^6$) | $\Delta$ ($10^6$) |
|---|---|---|---|---|---|---|
| | | | Figure 7 | | | |
| | 0.05 | 40 | 2.01 | 33510 | 2.23 | |
| T=447 K | 0.10 | 72 | 6.51 | 195432 | 13.03 | 10.80 |
| | 0.15 | 102 | 13.07 | 555647 | 37.04 | 24.01 |
| P=27.8 torr | 0.20 | 125 | 19.63 | 1022654 | 68.18 | 31.14 |
| | 0.25 | 128 | 20.59 | 1098066 | 73.20 | 5.02 |
| | | | Figure 8 | | | |
| | 0.05 | 48 | 2.90 | 57906 | 3.86 | |
| T=519 K | 0.10 | 68 | 5.81 | 164636 | 10.98 | 7.12 |
| | 0.15 | 93 | 10.87 | 421160 | 28.08 | 17.10 |
| P=29.8 torr | 0.20 | 122 | 18.70 | 950776 | 63.39 | 35.31 |
| | 0.25 | 128 | 20.59 | 1098066 | 73.20 | 9.81 |